RESEARCH ARTICLE | JULY 17 2023

Study on the energy-focusing mechanism of spatial bubble clusters ⊘

Zhendong Bian (卞真东) ⓘ ; Tezhuan Du (杜特专) ✉ ⓘ ; Jianlin Huang (黄剑霖) ⓘ ; Jingzhu Wang (王静竹) ⓘ ;
Yiwei Wang (王一伟) ⓘ

Check for updates

View Online

Export Citation

08 April 2024 02:56:14

AIP Publishing

Study on the energy-focusing mechanism of spatial bubble clusters

View Online   Export Citation   CrossMark

Zhendong Bian (卞真东),[1,2] Tezhuan Du (杜特专),[1,2,a] Jianlin Huang (黄剑霖),[2,3] Jingzhu Wang (王静竹),[1,2]
and Yiwei Wang (王一伟)[1,2,3]

AFFILIATIONS

[1]School of Engineering Science, University of Chinese Academy of Sciences, Beijing 100049, China
[2]Key Laboratory for Mechanics in Fluid Solid Coupling Systems, Institute of Mechanics, Chinese Academy of Sciences,
 Beijing 100190, China
[3]School of Future Technology, University of Chinese Academy of Sciences, Beijing 100049, China

[a]Author to whom correspondence should be addressed: dutezhuan@imech.ac.cn

ABSTRACT

Cavitation research has important implications in fields such as mechanical drag reduction, material processing, and new medical device development. Bubble cluster formation, development, and collapse are critical steps in the cavitation process. High-precision numerical simulations have shown that the collapse of bubble clusters exhibits a characteristic energy focusing from the outside to the inside. This study proposes a focus-type model for the energy transfer in bubble clusters to analyze the formation mechanism of collapse pressure and improve the accuracy of quantitative predictions. The model comprises multiple bubbles (α) radiating energy and a bubble (β) receiving energy. Through numerical simulation, the energy transfer law during bubble interaction is studied, showing that relative energy transfer decreases as the dimensionless distance increases, which corresponds with the theoretical model. The study further analyses the relationship between energy transfer in basic and composite bubble cluster structures. Additionally, the study observed the pressure focusing effect of the bubble clusters and found a strong correlation between the focusing effect and dimensionless distance.

I. INTRODUCTION

Cavitation is ubiquitous in nature and plays an important role in several scientific and engineering fields. For example, in turbine machineries, cavitation effects are widely used to reduce the friction and drag of turbine blades, thereby improving the operational efficiency.[1,2] In materials processing, bubble flow impacting material surfaces can enhance the mechanical properties of the materials.[3–6] In materials and equipment cleaning, the cavitation effect generated by ultrasound is widely used for cleaning semiconductor materials, metal parts, and industrial equipment.[7–10] In medical technologies, microbubbles generated by high-frequency ultrasound can be used as a non-invasive treatment method in operations such as stone fragmentation, tumor ablation, and imaging, without necessarily cutting into important organs such as the kidneys, thereby considerably reducing the surgical risks and patient discomfort.[11–14] Researchers have found that the complex dynamic characteristics of bubble clusters are the main reason for the occurrence of cavitation effects.[15–17] Hence, the study and application of bubble cluster dynamics have become one of the most important topics in the field of cavitation science. As the application areas for cavitation effects continue to expand and deepen, research in this direction has become increasingly essential.

The study of bubbles can be traced back to Besant,[18] who established a single bubble model in 1859 and successfully predicted the period of the bubbles. Furthermore, Rayleigh[19] established a mathematical model for a spherical bubble based on the assumption of non-viscous and incompressible fluids and predicted the pressure of the bubbles. Plesset[20] further analyzed the influence of liquid viscosity and surface tension on bubble motion based on Rayleigh's work and found that viscosity reduces the size of the bubble expansion, while surface tension affects the period of the bubble motion. Researchers[21,22] have also studied the effect of viscosity on the bubble motion by replacing water solutions with other liquid solutions such as kerosene and silicone oil. When the bubbles violently collapse, the velocity of the bubble boundary is of the same order of magnitude as that of the sound speed c in water, thereby resulting in strong pressure waves during the bubble expansion.[23–25] Bubble models tend to be developed based on an assumption of incompressibility. To address the problem of compressibility, several researchers, such as Keller and Kolodner,[26] Keller

08 April 2024 02:56:14

and Miksis,[27] Gilmore,[28] Trilling,[29] Keller and Kolodner,[26] Prosperetti and Lezzi,[17] and Lezzi and Prosperetti,[30] have proposed different models based on the weakly compressible and perturbation theory. Another topic of interest is the interaction between bubbles and complex boundary conditions. Some researchers[31–38] studied the interaction between a solid wall and single bubble and found that bubbles undergo non-spherical deformation and induce liquid jets toward solid walls. Others, such as Pearson et al.,[39] Wang et al.,[40] Zhang et al.,[41] Trummler et al.,[42] and Li et al.,[43] studied bubbles near the free surfaces and found that such bubbles produce high-speed liquid jets away from the free surface direction. Furthermore, Bremond et al.[44] and Harkin et al.,[45] investigated the interactions among few bubbles and analyzed the influence of pressure waves and jet flows on the translation and spherical oscillations of the bubbles.

The pressure wave generated by the bubble expansion and high-speed jet induced by non-spherical collapse are the main causes of the structural damage of the bubbles. Additionally, high-precision numerical simulations have shown that the arrangement of the bubble clusters has a close relationship with the geometric focusing effect during bubble collapse, wherein the pressure peak and energy propagate from the outside to the inside, thereby generating extremely high collapse pressure near the center of the bubble cluster.[46–48] Currently, different theoretical models for bubble interaction are based on assumptions of non-rotation and spherical bubbles in the construction of the potential function. For cases with small numbers of bubbles, Zhang et al.[49] proposed a unified theory of bubble dynamics that can accurately predict the characteristics of bubble oscillation, migration, and collapse pressure. For larger numbers of bubbles, the Lagrangian method is usually adopted to first solve for the potential function and derive the total kinetic and potential energies of the entire field, after which substitutions are made into the equations to calculate the pulsation and translation of any bubble.

Owing to the random distributions of the bubble clusters, an accurate theoretical formula for the potential function cannot be obtained. Hence, approximation methods are usually used to construct the potential function to replace the real potential function.[50–53] Among these approximation methods, using the series methods to approximate the potential function is one of the most common. For example, Ilinskii et al.[54] used a Taylor series, whereas Kurihara et al.[55] used a Bessel series. Although this method simplifies the difficulty of solving the bubble cluster, there are limitations in analyzing the problems and processes that involve compressibility, such as bubble deformation. Hence, this study proposes a focus-type model of the energy transfer in bubble clusters based on an approximate solution of the potential function, with the aim of evaluating and describing the interaction between the bubble clusters, and exploring the energy-focusing characteristics of the focus effect in the bubble cluster collapse process.

II. RESEARCH METHODS

This study examines the characteristics of energy and pressure aggregation toward the center of a bubble cluster during its collapse process and constructs a concentrated bubble cluster energy transfer model. Here, numerical simulations are conducted to analyze this model.

A. Focused bubble cluster energy transfer model

The focused bubble energy transfer model is shown in Fig. 1. In the model, the blue and red spheres represent the energy-radiating bubble (α-bubble) and energy-absorbing bubbles (β-bubble). The initial radius of these two types of bubbles completely equals in the simulation.

If the flow around the bubbles is irrotational and inviscid, then there exists a potential function ϕ that satisfies Eq. (1)

$$\nabla^2 \phi = 0. \tag{1}$$

Based on the spherical-bubble assumption, for any bubble i, Eq. (2) must be satisfied at the boundary, where u_i and $\dot{R}_i$ represent the translational velocity and pulsation velocity of the bubble, respectively,

$$\frac{\partial \phi}{\partial r_i} = \dot{R} + U_i \cdot n_i. \tag{2}$$

Approximation methods are usually used to solve the potential function ϕ. Ilinskii et al.[54] integrated Eq. (2) to obtain a first-order potential function ϕ_{0i} applicable to any bubble

$$\phi_{0i} = -\frac{R_i^2}{r_i}\dot{R}_i - \frac{R_i^3}{2r_i^2}U_i \cdot n_i. \tag{3}$$

Adding the first-order potential functions over the entire field yields,

$$\phi_0 = \sum_i \phi_{0i}. \tag{4}$$

Expanding ϕ_0 near the ith bubble yields,

$$\phi_0(r_i) = \phi_{0i}(r_i) + \sum_{k \neq i} \phi_{0k}(r_{ki} + r_i)$$
$$= \phi_{0i}(r_i) + \sum_{k \neq i}\left[\phi_{0k}(r_{ki}) + c_{ki} \cdot r_i + \cdots\right]. \tag{5}$$
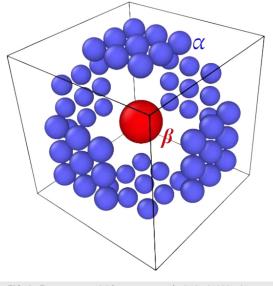

FIG. 1. Focus-type model for energy transfer in the bubble cluster.

Here, $c_{ki} \cdot r_i$ represents the first-order term of the Taylor series, of which the higher-order terms are ignored. Hence, ϕ_0 no longer satisfies Eq. (1) and needs to be supplemented. To do this, Ilinskii *et al.* used a construction method similar to ϕ_0 to obtain an approximate substitute function ϕ_1 for the higher-order terms and later added both simultaneously to obtain an approximate solution to the potential function, that is,

$$\phi = \phi_0 + \phi_1. \quad (6)$$

It is worth noting that the accuracy of the approximate solution to ϕ obtained using this method can reach the fourth order.

$$K = -\frac{\rho}{2} \sum_i \int_{S_i} \left(\dot{R} + U_i \cdot n_i \right) \phi dS_i. \quad (7)$$

Furthermore, the potential function ϕ is substituted into Eq. (7), and an approximate solution to the total field kinetic energy level of the focused bubble array near the receiving bubble is obtained. The specific form is expressed by the following equation:

$$K = K_1\left(R_i, \dot{R}_i\right) + K_2\left(R_i, R_k, \dot{R}_i, \dot{R}_k, U_i, U_k, r_{ik}\right)$$
$$+ K_3\left(R_i, R_j, R_k, \dot{R}_i, \dot{R}_k, r_{ik}, r_{jk}\right). \quad (8)$$

Here, K_1 represents the kinetic energy generated by the ith bubble itself

$$K_1\left(R_i, \dot{R}_i\right) = 2\pi\rho \left[\sum_i R_i^3 \dot{R}_i^2 + \frac{1}{6} \sum_i R_i^3 U_i^2 \right], \quad (9)$$

K_2 represents the change in the kinetic energy caused by the interaction between the kth and ith bubble expressed as follows:

$$K_2 = \sum_{i,k}^{i \neq k} \frac{R_i^2 \dot{R}_k^2}{r_{ik}} R_i \dot{R}_k + \frac{1}{2} \sum_{i,k}^{i \neq k} \frac{R_i^2 R_k^2}{r_{ik}^2} \left[R_i \dot{R}_k (U_i \cdot n_{ik}) + R_k \dot{R}_i (U_k \cdot n_{ki}) \right]$$
$$+ \frac{1}{4} \sum_{i,k}^{i \neq k} \frac{R_i^3 R_k^3}{r_{ik}^3} \left[(U_i \cdot U_k) - 3(U_i \cdot n_{ik})(U_k \cdot n_{ik}) \right], \quad (10)$$

and K_3 represents the effect of other bubbles (excluding the ith and kth bubbles) on the interaction between the kth and ith bubble expressed as follows:

$$K_3 = \frac{1}{2} \sum_{i,j,k}^{k \neq i,j} \frac{R_i^2 R_j^2 R_k^3}{r_{ik}^2 r_{jk}^2} \dot{R}_i \dot{R}_j (n_{ik} \cdot n_{jk}). \quad (11)$$

The preceding equations show the method of series expansion to obtain an approximate solution for the kinetic energy based on the assumption of a multi-bubble system, with the bubble at position i as the focus (assuming that there are no other bubbles between the receiving and radiating bubbles). However, the conventional Lagrangian method ignores the compressibility of the liquid when calculating the motion of the bubble cluster. As such, directly using this method to solve the motion of each bubble in the bubble cluster may result in large errors. To solve this problem, we combine the solution derived thus far with the potential function method to develop an energy transfer model suitable for a focused bubble cluster. In the numerical calculation process of the model, we set a reasonable

operating range to ensure that the surrounding energy-radiating bubbles α do not produce a jet after the central receiving bubble β reaches its maximum receiving energy. At this point, the α bubble maintains a spherical shape, whereas the central β bubble shrinks to its minimum volume. Through the aforementioned processing method, we can use the potential function method to study the energy transfer between the bubbles and reduce the errors. However, from the perspective of energy conservation, when a surrounding bubble α expands, most of its energy is converted into the kinetic energy of the liquid. Furthermore, the liquid with the kinetic energy generates pressure on the surface of the central bubble β, thereby converting it into the energy of the central bubble β. Hence, it is assumed that the kinetic energy $K(t)$ and energy δ of the central bubble β can be expressed by the following linear relationship:

$$K(t) = c \cdot \delta(t + \tau_0). \quad (12)$$

Equation (12) describes the conversion of the kinetic energy into the potential energy of the central bubble β through a proportional coefficient c and a time delay τ_0. This means that the kinetic energy is converted into the potential energy of the central bubble β proportionally by c, but this conversion process takes time τ_0 to complete. Some researchers have studied the time-phase difference problems related to the bubble research.[56,57] However, we focus more on energy transfer here and thus approximate that $\tau_0 \approx 0$. From this, we can obtain the expression for the relative potential energy ε_k of the central bubble β,

$$\varepsilon_K = \frac{\delta(t)}{p_\beta(0) V_\beta(0)}. \quad (13)$$

Combining Eqs. (8), (12), and (13) yields a rank expression for the relative potential energy of the central bubble β in the form

$$\varepsilon_K = \sum_{i,k}^{i \neq k} \frac{a_{1i}}{r_{ik}} + \sum_{i,k}^{i \neq k} \frac{a_{2i}}{r_{ik}^2} + \sum_{i,k}^{i \neq k} \frac{a_{3i}}{r_{ik}^3} + \sum_{i,k}^{i \neq k} \frac{a_{4i}}{r_{ik}^2 r_{jk}^2}, \quad (14)$$

where a_{1i}, a_{2i}, a_{3i}, and a_{4i} are undetermined coefficients, whereas r_{ik} and r_{jk} represent the distances between the bubbles i and j, and j and k, respectively. Owing to the nature of the energy transfer model, the central bubble β does not radiate energy. Hence, the kinetic energy caused by the central bubble is zero, that is,

$$\varepsilon_{K1} = 0. \quad (15)$$

The contribution in terms of the relative potential energy caused by the influence of the kth bubble on the ith bubble is expressed as follows:

$$\varepsilon_{K2} = \sum_{i,k}^{i \neq k} \frac{a_{1i}}{r_{ik}} + \sum_{i,k}^{i \neq k} \frac{a_{2i}}{r_{ik}^2} + \sum_{i,k}^{i \neq k} \frac{a_{3i}}{r_{ik}^3}. \quad (16)$$

The contribution in terms of the relative potential energy caused by the influence of the third bubble j on the relationship between bubble k and i is expressed as follows:

$$\varepsilon_{K3} = \sum_{i,k}^{i \neq k} \frac{a_{4i}}{r_{ik}^2 r_{jk}^2}. \quad (17)$$

When there are only two bubbles present, Eq. (14) simplifies to

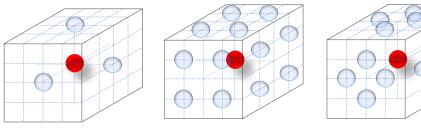**(a) First arrangement**　　**(b) Second arrangement**　　**(c) Third arrangement**

FIG. 2. Three symmetrical arrangements of basic bubble cluster: (a) first arrangement; (b) second arrangement; and (c) third arrangement.

$$\varepsilon_{K^*} = \frac{a_1}{r} + \frac{a_2}{r^2} + \frac{a_3}{r^3}. \tag{18}$$

Furthermore, when $a_1 = a_3 \approx 0$, the relative potential energy is inversely proportional to the square of the distance, which corresponds with previous research results.[58] Hence, Eq. (14) is more general.

Equation (14) shows that the relative potential energy of the central bubble is related to the initial energy of the radiating bubbles, the distance between the bubbles, and their spatial positions. In this study, we aim to investigate this characteristic further and explore the effects of the multiple bubble arrangements. To achieve this, we decompose the bubble cluster in Fig. 1 into three basic structural arrangements and perform numerical validation. Here, we refer to the bubble cluster in Fig. 1 as the composite bubble cluster and distinguish the three basic arrangements, visualized in Fig. 2, by their serial numbers. In Fig. 2, the red and blue spheres represent the receiving and radiating bubbles, respectively. The upper 3D image shows the spatial arrangement of the bubble cluster, whereas the lower image illustrates the position relationship between the radiating bubbles α on the cubic surface. Hence, for our approach, we first obtain the relative energy received by the center bubble in the composite bubble cluster. Furthermore, we calculate the relative energy of the three decomposed bubble clusters and center bubbles under identical dimensionless distance conditions. Furthermore, their results are superimposed. Finally, the obtained numerical results are compared to those of the numerical simulation for the composite bubble clusters.

In the numerical simulation, we also implement a dimensionless approach on the model and study the energy transfer between the bubbles by varying the dimensionless distance d expressed as follows:

$$d = \frac{l}{2R}, \tag{19}$$

where l represents the edge length of the cube and R the initial volume of the bubble.

The different bubble cluster structures differ mainly in the distance between the radiating bubbles on the cube face at a similar dimensionless distance d. This factor leads to differences in the relative received energy of the center bubble. To compare the effects of the different bubble cluster structures, we normalize the distances between the radiating bubbles in the different structures, as shown in Fig. 3.
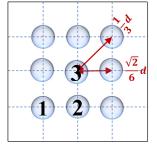
Of these diagrams, Fig. 3(a) portrays the hindrance effect between α the bubbles in the composite structure, Fig. 3(b) the hindrance effect between α the bubbles in the second basic structure, and Fig. 3(c) the hindrance effect between α the bubbles in the third basic structure. Thus, the relationship between the bubble positions in the basic arrangement and energy of the central bubble can be obtained. Similarly, both dimensionless distances between the radiating bubbles in the second and third types of the basic structures can be determined (there is only one radiating bubble on the surface of the first basic structure. There are no two extra dimensionless distances).
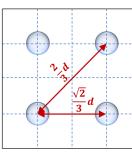
1. In the second type of basic arrangement, the distances between the adjacent and diagonal bubbles are as follows:

$$d_{\alpha 2} = \frac{1}{3}d, \quad d'_{\alpha 2} = \frac{\sqrt{2}}{3}d. \tag{20}$$

2. In the third type of basic arrangement, the distances between the adjacent and diagonal bubbles are expressed as follows:

Inhibitory Effect

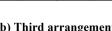**(a) Composite arrangement**　　**(b) Second arrangement**　　**(b) Third arrangement**

FIG. 3. Secondary dimensionless distance (distance between the α-bubbles) in the three types of bubble cluster arrangements. (a) Composite arrangement; (b) second arrangement; and (c) third arrangement.

$$d_{\alpha 3} = \frac{\sqrt{2}}{6} d, \quad d'_{\alpha 3} = \frac{1}{3} d. \tag{21}$$

By the substitution of the theoretical values of the dimensionless distances into the theoretical model Eq. (14), the theoretical formula for the relative energy received by the central bubble in each basic structure for the three bubble clusters can be obtained as follows:

- For the first basic structure,

$$\varepsilon_{K1} = 6\left(\frac{a_1}{d} + \frac{a_2}{d^2} + \frac{a_3}{d^3}\right). \tag{22}$$

- For the second basic structure ($d' = \frac{\sqrt{38}}{6} d$),

$$\varepsilon_{K2} = 24\left[\left(\frac{a_1}{d'} + \frac{a_2}{d'^2} + \frac{a_3}{d'^3}\right) + \left(\frac{2a_4}{d'^2 \times \left(\frac{\sqrt{2}}{3} d\right)^2} + \frac{a_5}{d'^2 \times \left(\frac{2}{3} d\right)^2}\right)\right],$$

$$= 24\left[\left(\frac{3\sqrt{10}a_1}{10d} + \frac{9a_2}{10d^2} + \frac{27\sqrt{10}a_3}{100d^3}\right) + \left(\frac{81a_4}{10d^4} + \frac{81a_5}{40d^4}\right)\right]. \tag{23}$$

- For the third basic structure ($d'' = \frac{\sqrt{10}}{3} d$),

$$\varepsilon_{K3} = 24\left[\left(\frac{a_1}{d''} + \frac{a_2}{d''^2} + \frac{a_3}{d''^3}\right) + \left(\frac{2a_4}{d''^2 \times \left(\frac{1}{3} d\right)^2} + \frac{a_5}{d''^2 \times \left(\frac{\sqrt{2}}{3} d\right)^2}\right)\right]$$

$$= 24\left[\left(\frac{3\sqrt{38}a_1}{19d} + \frac{36a_2}{38d^2} + \frac{54\sqrt{38}a_3}{361d^3}\right) + \left(\frac{81a_4}{19d^4} + \frac{81a_5}{38d^4}\right)\right]. \tag{24}$$

The principle behind the derivations of the aforementioned formulas is as follows: the relative potential energy of the central bubble in the basic bubble cluster is the linear superposition of the energy transmitted to the central bubble by all the radiating bubbles. Here, numerical simulations are used to fit the coefficients of the energy transfer model for the three basic structures. Furthermore, the energy transfer law of the composite bubble cluster is analyzed.

B. Numerical simulation methods

In this study, the compressibleInterFoam solver under the OpenFOAM framework is used for the numerical simulations, and the volume-of-fluid (VOF) method is used to capture the gas–liquid interface. The VOF method describes the changes in the gas–liquid interface based on solving the volume fraction transport equation, Eq. (25).[59] Here, u represents the velocity field, U_r the relative velocity between both phases, and p_l and p_a the pressures of the liquid phase and gas phase, respectively, as follows:

$$\frac{\partial \alpha_l}{\partial t} + \nabla \cdot (\alpha_l u) + \nabla \cdot (\alpha_l (1 - \alpha_l) U_r)$$

$$= \alpha_l (1 - \alpha_l)\left(\frac{1}{\rho_a}\frac{D\rho_a}{Dp_a} - \frac{1}{\rho_l}\frac{D\rho_l}{Dp_l}\right)\frac{Dp_l}{Dt} + \alpha_l \nabla \cdot u. \tag{25}$$

This method has advantages in terms of a high computational accuracy and fast calculation speed, and is widely used in fields such as hydraulics, environmental engineering, and geological engineering.[60–63]

In the numerical simulations, it is necessary to confirm the parameters of the gas and liquid state equation. In this study, the ideal gas state equation is used to describe the gas inside the bubbles, which is expressed as follows:

$$p_a V_a = nRT_a, \tag{26}$$

where V_L, T_b, and p represent the volume of the liquid, temperature of the liquid, and pressure, respectively. The state equation for pure water is expressed as follows:

$$\frac{1}{\rho_l} = 0.001\,278 - 2.1055 \times 10^{-6}T_l + 3.9689 \times 10^{-9}T_l^2$$

$$- 4.3772 \times 10^{-13}p_l + 2.0225 \times 10^{-13}p_l T_l, \tag{27}$$

where T_l represents the temperature of the liquid. Other parameters used in the numerical process are shown in Table I.

To ensure the accuracy of the computational results, appropriate boundary conditions need to be set at the inlet and outlet of the computational domain (away from the bubbles). In this study, the velocity boundary condition is set to pressureInletOutletVelocity, which allows the velocity to freely adjust its component perpendicular to the boundary. Additionally, to eliminate the influence of the pressure wave reflection at the boundary on the computational results, the pressure inlet and outlet boundaries are set to waveTransmissive.[64]

Figure 4 shows a diagram of the meshing of the computational domain. The snappyHexMesh was used to generate the mesh with five levels of refinement. The ratio of the size of the outermost mesh element to the size of the innermost mesh element was $2^5 : 1$, and the bubble was located at the center of the mesh refinement region. The size of the domain during the calculation was $60 \times 60 \times 60\,\text{mm}^3$, and the size of the core region was $10 \times 10 \times 10\,\text{mm}^3$. During the calculation, the coarse and fine mesh comprised 1.33×10^6 and 32.8×10^6 mesh elements, respectively, with a length of 0.0293 mm per unit mesh element within the computational domain.

Furthermore, we used a single bubble with an initial radius of 0.6 mm and internal pressure of 0.6 MPa for the simulation, and the results are shown in Fig. 5. During most of the bubble pulsation phases, the mesh is able to accurately capture changes in the bubble radius (the error in bubble radius, in both numerical and theoretical, is kept within a maximum tolerance of 5%), which is already sufficient to fulfill the requirements of the bubble cluster energy transfer model.

Finally, we validate our method for capturing bubble deformation and jet morphology using experimental and numerical results of a

TABLE I. Parameters used in the numerical simulation of the double bubbles.

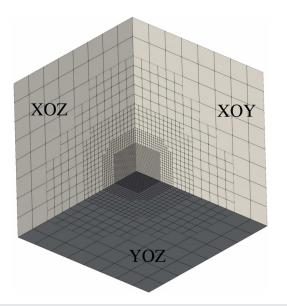|	Unit	Air	Liquid	Mixture
Specific heat capacities (C_p)	J/(mol K)	1007	$\cdots$	$\cdots$
Specific heat capacities (C_v)	J/(mol K)	$\cdots$	4195	$\cdots$
Dynamic viscosity	Pa s	$\cdots$	$\cdots$	$\cdots$
Prandtl number	1	0.7	7	$\cdots$
Heat of formation	J/mol	0	0	$\cdots$
Surface tension coefficient	N/m	$\cdots$	$\cdots$	0.07
Ideal gas constant	J/(mol K)	$\cdots$	$\cdots$	8.31
Gravity acceleration	m/s^{-2}	$\cdots$	$\cdots$	0.00

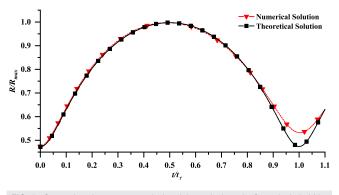FIG. 4. Schematic diagram of the grid in a one-eighth computational domain.

FIG. 5. Comparison between numerical and theoretical results for a single bubble.

bubble near a wall. The schematic diagram of this condition can be seen in Fig. 6.

We calculated the cases with dimensionless distance d of 1.25 and 1.75, and the computed results are shown in Fig. 7. The error in

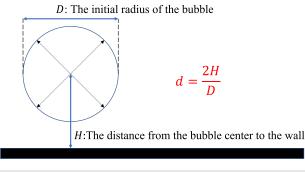
FIG. 6. Definition of dimensionless parameters.

bubble volume, in both numerical and experimental aspects, is kept within a maximum tolerance of 3%.

III. RESULTS AND ANALYSIS

A. Analysis of pressure characteristics

First, we analyzed the pressure characteristics during the evolution process of the bubble cluster. Taking the energy transfer model of the first-type bubble cluster as an example, we extracted the results of the bubble cluster motion at the eighth time step, as shown in Fig. 8. The white outline in the figure represents the boundary of the bubble. In analyzing the pressure transmission, we used relative pressure, which is obtained by dividing the actual pressure by the ambient pressure.

Furthermore, we conducted a thorough investigation of the pressure of the central bubble. Specifically, we observed the pressure–time curve of the central bubble in the third type of basic bubble cluster (the pressure characteristics of the central bubble in the three types of basic bubble clusters are similar) and plotted the pressure curves at different non-dimensional distances in Fig. 9. Here, P_{sat} represents the ambient pressure, and the bubble collapse time varies at different non-dimensional distances, with $t_\tau = 10^{-5}$. Our research results show that the relative energy received by the central bubble is positively correlated with the relative pressure inside the bubble. Figure 9 shows that the peak pressure in the central bubble increases with the decrease of nondimension distance, and the peak pressure can reach 800 times the ambient pressure. Additionally, as the non-dimensional distance increases, the time when the pressure peak appears also shifts backward, that is, the collapse time of the central bubble is delayed. We believe that these research results are very helpful for a deeper understanding of the energy transfer characteristics of the focused bubble clusters, and also provide guidance in terms of exploring the evolution rules of the bubble clusters.

B. Analysis of energy transmission

In the numerical simulation of the focused bubble clusters, we adopted a method of varying the dimensionless distance to calculate the energy received by the central bubble in four different bubble cluster arrangements. First, we verified the three basic bubble cluster arrangements and calculated the relative energy transferred from each α bubble to the central β bubble on average for each arrangement. The specific results are shown in Table II. Here, ε_1^*, ε_2^*, ε_3^*, and ε^* represent the average relative energies transferred from a single α bubble to the central β bubble in the first, second, and third types of basic bubble cluster arrangements and the composite bubble cluster arrangement, respectively. The results show that the relative energy transferred by each α bubble to the central bubble decreases with an increase in the number of α bubbles in the cluster arrangement. Additionally, the average energy transferred from each bubble to the central bubble decreases as the dimensionless distance increases.

Based on the theoretical models (15)–(17), we calculated the average energy transferred from each radiating bubble to the center bubble for the three basic bubble arrangements and obtained the corresponding fitting parameters, which are expressed by Eqs. (28)–(30), respectively,

$$\varepsilon_{K1}^* = \frac{1.466}{d} + \frac{1.000}{d^2} + \frac{0.920}{d^3} + 0.099, \qquad (28)$$

(a) $d = 1.25$						
$Time(ms)$	0.45	0.85	1.25	1.65	2.10	2.50
$R_e(mm)$	8.79	11.28	12.28	11.78	9.57	4.71
$R_s(mm)$	8.72	11.45	12.36	11.98	9.51	5.00

(b) $d = 1.75$						
$Time(ms)$	0.45	0.85	1.25	1.65	2.10	2.50
$R_e(mm)$	8.64	11.14	12.93	11.28	8.71	3.78
$R_s(mm)$	8.80	11.45	12.01	11.51	8.96	4.13

FIG. 7. Experimental results vs OpenFOAM results: (a) $d = 1.25$; and (b) $d = 1.75$. Left side represents experimental data, and right side represents simulation results. The maximum bubble radius in the experiments was 12 mm.

$$\varepsilon_{K2}^* = \frac{0.972}{d} + \frac{0.444}{d^2} + \frac{0.516}{d^3} + \frac{0.815}{d^4} + \frac{0.118}{d^5} + 0.188, \quad (29)$$

$$\varepsilon_{K3}^* = \frac{0.994}{d} + \frac{0.460}{d^2} + \frac{0.523}{d^3} + \frac{0.818}{d^4} + \frac{0.119}{d^5} + 0.156. \quad (30)$$

The fitting results are shown in Fig. 10. Here, the calculated and theoretical results for the relative energy transferred from each bubble to the central bubble, with respect to the increases in the dimensionless distance, show a similar trend; that is, the relative energy transferred from each bubble to the central bubble decreases as the dimensionless distance increases.

Furthermore, we investigated the energy transfer pattern of the central bubble in the composite bubble cluster arrangement by varying the dimensionless distance d. To better visualize the results, we present

the calculated results for the four types of bubble clusters together in Fig. 11. The results show that increasing the dimensionless distance also leads to a decrease in the relative energy received by the central bubble in the composite bubble cluster structure. Furthermore, by comparing the calculated results for the second and third types of basic bubble clusters, we can conclude that when the distance between α bubbles is reduced, the canceling effect between neighboring α bubbles is increased, thus hindering the energy transfer from the surrounding bubbles to the central bubble. When the dimensionless distance is small ($d < 3.6$), the strong interaction between α bubbles causes a considerable deformation of the bubbles, which invalidates our assumptions. Hence, the fitting data range for the composite bubble cluster is limited to $d > 3.6$. The obtained fitting results are as follows:
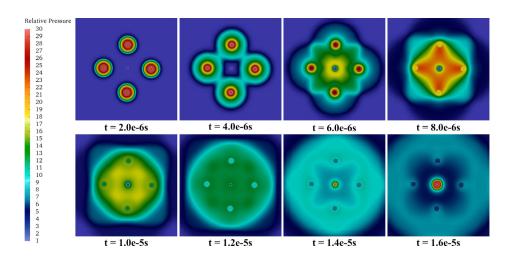

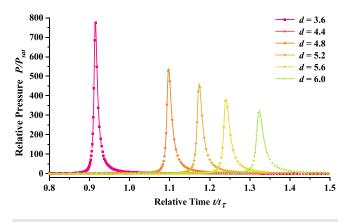**FIG. 8.** Flow field analysis of the first-type basic cluster.

FIG. 9. Time-dependent variation of the relative pressure in the central bubble of the third-class basic foam cluster.

TABLE II. Variation of the average energy transferred from a single α bubble to a β bubble in terms of the dimensionless distance for the three basic bubble arrangements.

d	3.2	3.6	4.0	4.4	4.8	5.0	5.2	5.6	6.0
ε_1^*	0.68	0.6	0.55	0.49	0.45	0.44	0.43	0.39	0.38
ε_2^*	0.55	0.51	0.48	0.44	0.42	0.4	0.39	0.38	0.37
ε_3^*	0.53	0.48	0.45	0.42	0.4	0.37	0.36	0.35	0.34
ε^*	0.44	0.43	0.41	0.38	0.35	0.34	0.34	0.32	0.31

$$\varepsilon = \frac{24.870}{d} + \frac{81.844}{d^2} + \frac{55.713}{d^3} + \frac{26.787}{d^4} + \frac{11.528}{d^5} + 9.715. \quad (31)$$

Here, we directly superimpose the calculation results for the three basic bubble cluster arrangements and compare the superimposed result with the numerical calculation result for the composite bubble cluster arrangement, as shown in Fig. 12.

The calculation results show that when $3.6 < d < 5.6$, the relative error between the energy transferred from the radiation bubbles to the central bubble in the basic bubble structure and that in the
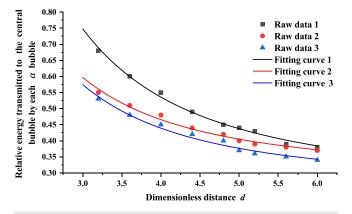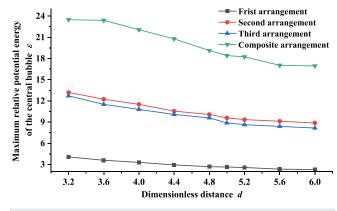

FIG. 11. Relationship between the energy received by the central bubble and dimensionless distance d for four types of bubble cluster arrangements.

composite bubble structure does not exceed 20%. This helps to approximately estimate the energy of the central bubble in a known structure when the bubble cluster collapses. To describe the difference E_u between the composite bubble cluster and superimposed bubble cluster, we assume that they satisfy the following relationship:

$$E(d) = E_1(d) + E_2(d) + E_3(d) - E_u(d), \quad (32)$$

where E_1, E_2, and E_3 represent the energy received by the central bubble in the three basic bubble arrangements, respectively, whereas E represents the energy received by the central bubble in the combined bubble arrangement. The difference $E_u(d)$ reflects the non-linear interaction between bubble clusters. By substituting the models (28)–(31) into (32), we obtain the expression for $E_u(d)$ $(d > 3.6)$,

$$E_u(d) = \frac{31.110}{d} - \frac{54.148}{d^2} - \frac{25.257}{d^3} + \frac{12.405}{d^4} - \frac{5.84}{d^5} - 0.865. \quad (33)$$

We conducted an analysis to investigate the decreasing then increasing trend of the E_u with increasing dimensionless distance. Given the characteristics of the focused structure model, there are two

FIG. 10. Average relative energy received by the center bubble as a function of the dimensionless distance d for each type of basic bubble cluster.
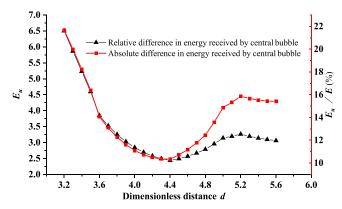

FIG. 12. Evolution of the difference in the energy received by the central bubble between the composite bubble clusters and overlapped bubble clusters as a function of dimensionless distance d.

mechanisms that affect the transfer of energy from the surrounding energy-radiating bubbles to the central bubble, as shown in Fig. 13. Both mechanisms are explained as follows:

1. If the spacing between the α bubbles is kept constant while that between the α bubbles and β bubbles is increased, then in this case, the α bubbles will decrease their energy transfer to the central bubble, thereby resulting in a weakened energy transfer.
2. If the spacing between α and β bubbles is kept constant while the spacing between α bubbles is increased, then in this case, the non-linear resistance is weakened, and the energy transfer from the α bubbles to the central bubble is increased, thereby resulting in strengthened energy transfer.

The combined action of both mechanisms results in very complex characteristics for the bubble clusters during the collapse process. Hence, it is not possible to simply linearly superimpose the numerical results of the basic bubble cluster to fit the energy transfer law of the complex bubble cluster. To accurately describe the influence of both mechanisms on the energy transfer of the bubble clusters, further quantitative research is needed.

IV. SUMMARY

The main contributions of this study are as follows:

1. A theoretical model for the energy received by the central bubble was constructed by combining potential functions and the principle of energy conservation.
2. Numerical simulations were conducted on three types of basic bubble clusters and composite bubble clusters to validate the theoretical model and determine its parameters.
3. The superposition relationship of the bubble clusters was analyzed, and the applicability of the superposition rules was explained under certain accuracy conditions.
4. The pressure characteristics of the bubble clusters were analyzed, thereby revealing the presence of considerable pressure focusing phenomena and identifying their influencing factors.

To elucidate the energy concentration characteristics in the collapse process of the natural bubble clusters, this study proposes a
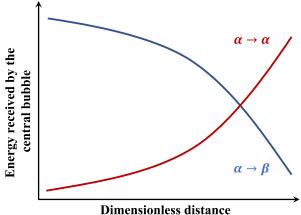

FIG. 13. Two mechanisms that cause different energy transfer patterns as the dimensionless distance changes.

focused structure model for the energy transfer of the bubble clusters. First, a potential function that satisfies the Laplace equation and bubble boundary conditions is constructed to describe the flow field. Based on the method by Ilinskii *et al.*, the potential function in the series form is obtained using the Taylor series near the receiving bubble, and the series expression of kinetic energy is derived via the substitution of the series form of the potential function into the kinetic energy equation. By assuming that kinetic energy can be converted into the energy of the central bubble based on certain rules, we indirectly derive the energy transferred from the radiating bubbles to the central bubble based on energy conservation.

First, we conducted an analysis of the pressure characteristics of the central bubble. The results reveal the presence of considerable pressure focusing the effects within the bubble cluster, closely correlated with the dimensionless distance. As the dimensionless distance increases, the pressure focusing effect weakens, and the peak occurs with a time delay.

To verify the accuracy of the model, we designed four different arrangements of the bubble clusters and conducted multiple numerical simulations with variations in the dimensionless distance to study the energy received by the central bubble in the three basic bubble cluster arrangements. The numerical results show that the relative energy received by the basic bubble cluster decreases as the dimensionless distance increases, which corresponds with the theoretical prediction. We used the numerical results to fit the theoretical model and obtained the fitting parameters. Additionally, we analyzed the superposition law between the different basic bubble cluster arrangements. Under an accuracy requirement in that the error should not exceed 20%, the numerical results for the composite bubble cluster can be regarded as the linear superposition of the numerical results for the basic bubble cluster.

Finally, we also analyzed the sources of the error and found that the error came mainly from the non-linear effects between the bubbles. Specifically, when the distance between α–α bubbles remains unchanged while the distance between α–β bubbles is increased, the energy of the central bubble decreases. However, when the distance between α–β bubbles remains unchanged while the distance between α–α bubbles is increased, it reduces the non-linear resistance effect, thereby resulting in an increase in the energy of the central bubble.

AUTHOR DECLARATIONS
Conflict of Interest

The authors have no conflicts to disclose.

Author Contributions

Zhendong Bian: Resources (equal); Writing – original draft (lead); Writing – review & editing (equal). **Tezhuan Du:** Supervision (equal); Validation (equal); Writing – original draft (equal); Writing – review

& editing (equal). **Jianlin Huang:** Resources (supporting). **Jingzhu Wang:** Supervision (supporting). **Yiwei Wang:** Supervision (supporting).

DATA AVAILABILITY

The data that support the findings of this study are available within the article.

REFERENCES

[1]R. E. Arndt, "Cavitation in fluid machinery and hydraulic structures," Annu. Rev. Fluid Mech. **13**, 273 (1981).

[2]A. Vacca, R. Klop, and M. Ivantysynova, "A numerical approach for the evaluation of the effects of air release and vapour cavitation on effective flow rate of axial piston machines," Int. J. Fluid Power **11**, 33 (2010).

[3]Z. Wang, H. Cheng, and B. Ji, "Numerical prediction of cavitation erosion risk in an axisymmetric nozzle using a multi-scale approach," Phys. Fluids **34**, 062112 (2022).

[4]A. Świetlicki, M. Szala, and M. Walczak, "Effects of shot peening and cavitation peening on properties of surface layer of metallic materials—A short review," Materials **15**, 2476 (2022).

[5]C. Prado, F. Antunes, T. Rocha, S. Sánchez-Muñoz, F. Barbosa, R. Terán-Hilares, M. Cruz-Santos, G. Arruda, S. da Silva, and J. Santos, "A review on recent developments in hydrodynamic cavitation and advanced oxidative processes for pretreatment of lignocellulosic materials," Bioresour. Technol. **345**, 126458 (2022).

[6]J. Hofmann, C. Thiébaut, M. Riondet, P. Lhuissier, S. Gaudion, and M. Fivel, "Comparison of acoustic and hydrodynamic cavitation: Material point of view," Phys. Fluids **35**, 017112 (2023).

[7]C.-D. Ohl, M. Arora, R. Dijkink, V. Janve, and D. Lohse, "Surface cleaning from laser-induced cavitation bubbles," Appl. Phys. Lett. **89**, 074102 (2006).

[8]M. Dular, T. Griessler-Bulc, I. Gutierrez-Aguirre, E. Heath, T. Kosjek, A. K. Klemenčič, M. Oder, M. Petkovšek, N. Rački, M. Ravnikar et al., "Use of hydrodynamic cavitation in (waste)water treatment," Ultrason. Sonochem. **29**, 577 (2016).

[9]G. L. Chahine, A. Kapahi, J.-K. Choi, and C.-T. Hsiao, "Modeling of surface cleaning by cavitation bubble dynamics and collapse," Ultrason. Sonochem. **29**, 528 (2016).

[10]X. Zhong, J. Dong, M. Liu, R. Meng, S. Li, and X. Pan, "Experimental study on ship fouling cleaning by ultrasonic-enhanced submerged cavitation jet: A preliminary study," Ocean Eng. **258**, 111844 (2022).

[11]D. L. Miller, "Overview of experimental studies of biological effects of medical ultrasound caused by gas body activation and inertial cavitation," Prog. Biophys. Mol. Biol. **93**, 314 (2007).

[12]C. E. Brennen, "Cavitation in medicine," Interface Focus **5**, 20150022 (2015).

[13]Z. Izadifar, P. Babyn, and D. Chapman, "Ultrasound cavitation/microbubble detection and medical applications," J. Med. Biol. Eng. **39**, 259 (2019).

[14]P. Pfeiffer, M. Shahrooz, M. Tortora, C. M. Casciola, R. Holman, R. Salomir, S. Meloni, and C.-D. Ohl, "Heterogeneous cavitation from atomically smooth liquid–liquid interfaces," Nat. Phys. **18**, 1431 (2022).

[15]Z. Feng and L. Leal, "Nonlinear bubble dynamics," Annu. Rev. Fluid Mech. **29**, 201 (1997).

[16]A. Zhang, P. Cui, J. Cui, and Q. Wang, "Experimental study on bubble dynamics subject to buoyancy," J. Fluid Mech. **776**, 137 (2015).

[17]A. Prosperetti and A. Lezzi, "Bubble dynamics in a compressible liquid. Part 1. First-order theory," J. Fluid Mech. **168**, 457 (1986).

[18]W. H. Besant, A Treatise on Hydrostatics and Hydrodynamics (Deighton, Bell, 1859).

[19]L. Rayleigh, " VIII. On the pressure developed in a liquid during the collapse of a spherical cavity," London, Edinburgh, Dublin Philos. Mag. J. Sci. **34**, 94 (1917).

[20]M. S. Plesset, J. Appl. Mech. **16**, 277 (1949).

[21]E. B. Flint and K. S. Suslick, "The temperature of cavitation," Science **253**, 1397 (1991).

[22]G. P. W. Suyantara, T. Hirajima, A. M. Elmahdy, H. Miki, and K. Sasaki, "Effect of kerosene emulsion in $MgCl_2$ solution on the kinetics of bubble interactions with molybdenite and chalcopyrite," Colloids Surf., A **501**, 98 (2016).

[23]S. Li, D. van der Meer, A.-M. Zhang, A. Prosperetti, and D. Lohse, "Modelling large scale airgun-bubble dynamics with highly non-spherical features," Int. J. Multiphase Flow **122**, 103143 (2020).

[24]D. Fuster, C. Dopazo, and G. Hauke, "Liquid compressibility effects during the collapse of a single cavitating bubble," J. Acoust. Soc. Am. **129**, 122 (2011).

[25]Q. Wang, "Multi-oscillations of a bubble in a compressible liquid near a rigid boundary," J. Fluid Mech. **745**, 509 (2014).

[26]J. B. Keller and I. I. Kolodner, "Damping of underwater explosion bubble oscillations," J. Appl. Phys. **27**, 1152 (1956).

[27]F. R. Gilmore, California Institute of Technology, Hydrodynamics Laboratory, Report No. 26-4, Pasadena, CA (1952).

[28]J. B. Keller and M. Miksis, "Bubble oscillations of large amplitude," J. Acoust. Soc. Am. **68**, 628 (1980).

[29]L. Trilling, "The collapse and rebound of a gas bubble," J. Appl. Phys. **23**, 14 (1952).

[30]A. Lezzi and A. Prosperetti, "Bubble dynamics in a compressible liquid. Part 2. Second-order theory," J. Fluid Mech. **185**, 289–321 (1987).

[31]A. Shima, "Studies on bubble dynamics," Shock Waves **7**, 33 (1997).

[32]E. Brujan, A. Pearson, and J. Blake, "Pulsating, buoyant bubbles close to a rigid boundary and near the null final Kelvin impulse state," Int. J. Multiphase Flow **31**, 302 (2005).

[33]P. Gregorčič, R. Petkovšek, and J. Možina, "Investigation of a cavitation bubble between a rigid boundary and a free surface," J. Appl. Phys. **102**, 094904 (2007).

[34]S.-M. Li, A.-M. Zhang, Q. Wang, and S. Zhang, "The jet characteristics of bubbles near mixed boundaries," Phys. Fluids **31**, 107105 (2019).

[35]C. Lechner, W. Lauterborn, M. Koch, and R. Mettin, "Fast, thin jets from bubbles expanding and collapsing in extreme vicinity to a solid boundary: A numerical study," Phys. Rev. Fluids **4**, 021601 (2019).

[36]S. R. Gonzalez-Avila, F. Denner, and C.-D. Ohl, "The acoustic pressure generated by the cavitation bubble expansion and collapse near a rigid wall," Phys. Fluids **33**, 032118 (2021).

[37]T. Trummler, S. J. Schmidt, and N. A. Adams, "Effect of stand-off distance and spatial resolution on the pressure impact of near-wall vapor bubble collapses," Int. J. Multiphase Flow **141**, 103618 (2021).

[38]S.-M. Li, A.-M. Zhang, P. Cui, S. Li, and Y.-L. Liu, "Vertically neutral collapse of a pulsating bubble at the corner of a free surface and a rigid wall," J. Fluid Mech. **962**, A28 (2023).

[39]A. Pearson, E. Cox, J. Blake, and S. Otto, "Bubble interactions near a free surface," Eng. Anal. Boundary Elem. **28**, 295 (2004).

[40]Q. Wang, K. Yeo, B. Khoo, and K. Lam, "Nonlinear interaction between gas bubble and free surface," Comput. Fluids **25**, 607 (1996).

[41]S. Zhang, S. Wang, A. Zhang, and Y. Li, "Numerical study on attenuation of bubble pulse through tuning the air-gun array with the particle swarm optimization method," Appl. Ocean Res. **66**, 13 (2017).

[42]T. Trummler, S. H. Bryngelson, K. Schmidmayer, S. J. Schmidt, T. Colonius, and N. A. Adams, "Near-surface dynamics of a gas bubble collapsing above a crevice," J. Fluid Mech. **899**, A16 (2020).

[43]S.-M. Li, A.-M. Zhang, and N.-N. Liu, "Effect of a rigid structure on the dynamics of a bubble beneath the free surface," Theor. Appl. Mech. Lett. **11**, 100311 (2021).

[44]N. Bremond, M. Arora, C.-D. Ohl, and D. Lohse, "Controlled multibubble surface cavitation," Phys. Rev. Lett. **96**, 224501 (2006).

[45]A. Harkin, T. J. Kaper, and A. Nadim, "Coupled pulsation and translation of two gas bubbles in a liquid," J. Fluid Mech. **445**, 377–411 (2001).

[46]A. Tiwari, C. Pantano, and J. B. Freund, "Growth-and-collapse dynamics of small bubble clusters near a wall," J. Fluid Mech. **775**, R3 (2015).

[47]T. Du, Y. Wang, L. Liao, and C. Huang, "A numerical model for the evolution of internal structure of cavitation cloud," Phys. Fluids **28**, 077103 (2016).

[48]K. Maeda and T. Colonius, "Bubble cloud dynamics in an ultrasound field," J. Fluid Mech. **862**, 1105 (2019).

[49]A.-M. Zhang, S.-M. Li, P. Cui, S. Li, and Y.-L. Liu, "A unified theory for bubble dynamics," Phys. Fluids **35**, 033323 (2023).

[50]G. Contopoulos, "Infinite bifurcations, gaps and bubbles in Hamiltonian systems," Phys. D **8**, 142 (1983).

[51]T. B. Benjamin, "Hamiltonian theory for motions of bubbles in an infinite liquid," J. Fluid Mech. **181**, 349 (1987).

[52]S. A. Yi, V. Khudik, S. Y. Kalmykov, and G. Shvets, "Hamiltonian analysis of electron self-injection and acceleration into an evolving plasma bubble," Plasma Phys. Controlled Fusion **53**, 014012 (2011).

[53]K. Manohar, B. W. Brunton, J. N. Kutz, and S. L. Brunton, "Data-driven sparse sensor placement for reconstruction: Demonstrating the benefits of exploiting known patterns," IEEE Control Syst. Mag. **38**, 63 (2018).

[54]Y. A. Ilinskii, M. F. Hamilton, and E. A. Zabolotskaya, "Bubble interaction dynamics in Lagrangian and Hamiltonian mechanics," J. Acoust. Soc. Am. **121**, 786 (2007).

[55]E. Kurihara, T. A. Hay, Y. A. Ilinskii, E. A. Zabolotskaya, and M. F. Hamilton, "Model for the dynamics of two interacting axisymmetric spherical bubbles undergoing small shape oscillations," J. Acoust. Soc. Am. **130**, 3357 (2011).

[56]T. W. B. Kibble and A. Vilenkin, "Phase equilibration in bubble collisions," Phys. Rev. D **52**, 679 (1995).

[57]M. S. Longuet-Higgins, "Viscous streaming from an oscillating spherical bubble," Proc. R. Soc. London, Ser. A **454**, 725 (1998).

[58]Z. Bian, J. Wang, B. Yin, Y. Wang, R. Qiu, Y. Wang, and T. Du, "Studies on two-bubble energy transfer model with radiant-receiver structure," Acta Mech. Sin. **38**, 322099 (2022).

[59]I. Malgarinos, N. Nikolopoulos, M. Marengo, C. Antonini, and M. Gavaises, "VOF simulations of the contact angle dynamics during the drop spreading: Standard models and a new wetting force model," Adv. Colloid Interface Sci. **212**, 1–20 (2014).

[60]F. Garoosi, T. Merabtene, and T.-F. Mahdi, "Numerical simulation of merging of two rising bubbles with different densities and diameters using an enhanced volume-of-fluid (VOF) model," Ocean Eng. **247**, 110711 (2022).

[61]C. W. Hirt and B. D. Nichols, "Volume of fluid (VOF) method for the dynamics of free boundaries," J. Comput. Phys. **39**, 201 (1981).

[62]J. Klostermann, K. Schaake, and R. Schwarze, "Numerical simulation of a single rising bubble by VOF with surface compression," Int. J. Numer. Methods Fluids **71**, 960 (2013).

[63]M. Koch, C. Lechner, F. Reuter, K. Köhler, R. Mettin, and W. Lauterborn, "Numerical modeling of laser generated cavitation bubbles with the finite volume and volume of fluid method, using OpenFOAM," Comput. Fluids **126**, 71 (2016).

[64]W. Lauterborn, C. Lechner, M. Koch, and R. Mettin, "Bubble models and real bubbles: Rayleigh and energy-deposit cases in a Tait-compressible liquid," IMA J. Appl. Math. **83**, 556 (2018).

08 April 2024 02:56:14